

Theory of quasiparticle interference in Kitaev quantum spin liquids

Ammar Jahin,¹ Hao Zhang,^{1,2} Gábor B. Halász,^{3,4} and Shi-Zeng Lin^{1,2,5,*}

¹*Theoretical Divison, T-4, Los Alamos National Laboratory, Los Alamos, New Mexico 87545, USA*

²*CLNS, Los Alamos National Laboratory, Los Alamos, New Mexico 87545, USA*

³*Materials Science and Technology Divison, Oak Ridge National Laboratory, Oak Ridge, Tennessee 37831, USA*

⁴*Quantum Science Center, Oak Ridge, Tennessee 37831, USA*

⁵*Center for Integrated Nanotechnologies (CINT),
Los Alamos National Laboratory, Los Alamos, New Mexico 87545, USA*

(Dated: July 8, 2024)

We study quasiparticle interference (QPI) in the Kitaev quantum spin liquid (QSL) for electrons tunneling into the QSL. The local tunneling conductance around a spin vacancy or localized vison reveals unique features associated with fractionalized Majorana fermions, chargons, and visons. In certain parameter regimes, the single-spinon density of states and momentum dispersion can both be directly extracted from the tunneling conductance. Our results suggest that QPI is a promising tool for identifying the Kitaev QSL and its fractionalized excitations.

Introduction.—Quantum spin liquids (QSLs) are exotic phases of matter that avoid long-range ordering at zero temperature [1–5]. Rather, these phases are characterized by topological order associated with fractionalization, emergent gauge fields, and Abelian or non-Abelian anyonic quasiparticles. The interest in QSLs was initially driven by proposals linking them to high-temperature superconductivity upon doping [6]. Further understanding of QSLs showed that they have promising applications in topological quantum computation [7–9]. Despite such great interest and potential applications, a definitive experimental observation of these phases is still lacking after decades of search.

The Kitaev QSL [10] has recently been the subject of especially intensive study [11–13]. In this QSL, the spins are fractionalized into Majorana fermions and Z_2 gauge fields. Several materials, including $(\text{Na,Li})_2\text{IrO}_3$ [14–18] and $\alpha\text{-RuCl}_3$ [19–23] have been proposed to realize the Kitaev QSL with encouraging support from recent experiments. In particular, the half-integer-quantized thermal Hall conductivity expected [10] for the Kitaev QSL under a magnetic field has been observed [24–27], while evidence of fractionalization is reported from both Raman scattering and inelastic neutron scattering measurements [28–32]. Nevertheless, whether the Kitaev QSL is realized in these materials remains debated, calling for more conclusive signatures.

Quasiparticle interference (QPI) around scattering defects is generally a powerful probe of quantum materials [33–37] and emerges as an important tool for studying QSLs [38–43]. Indeed, recent scanning tunneling microscopy (STM) measurements on monolayer $\alpha\text{-RuCl}_3$ have reported distinctive oscillations in the local tunneling conductance around defects [44, 45]. Hence, there is an urgent need to develop a theory for QPI in the Kitaev QSL, which is crucial for both understanding the current experiments and predicting further signatures that can be used to identify Kitaev QSLs in future work.

To realize QPI in the Kitaev QSL, an electron from the

STM tip must tunnel directly into the QSL [see Fig. 1(a)], which is only possible when the bias voltage exceeds the Mott gap. This scenario is fundamentally different from previous theoretical setups where electrons were assumed to tunnel through the QSL [46–52]. In general, the injection of electrons or holes into the Kitaev QSL can give rise to several interesting phenomena such as superconductivity, kinetic ferromagnetism, and fractionalization of electrons, depending on the energy and density of the injected electrons or holes, as well as the details of the microscopic model [53–55]. In this work, we consider the scenario of spin-charge fractionalization where each electron tunneling into the QSL fractionalizes into a chargon and a spinon [see Fig. 1(a)].

Model.—We use the t - K model on a honeycomb lattice near half-filling to describe the Kitaev QSL phase with a doped electron,

$$H = -K \sum_{\langle \mathbf{r}, \mathbf{r}' \rangle} \hat{\sigma}_{\mathbf{r}}^{\alpha} \hat{\sigma}_{\mathbf{r}'}^{\alpha} - t \sum_{\langle \mathbf{r}, \mathbf{r}' \rangle} \sum_{\sigma} \left(\mathcal{P} d_{\mathbf{r}, \sigma}^{\dagger} d_{\mathbf{r}', \sigma} \mathcal{P} + \text{h.c.} \right) + \tilde{U} \sum_{\mathbf{r}} d_{\mathbf{r}, \uparrow}^{\dagger} d_{\mathbf{r}, \uparrow} d_{\mathbf{r}, \downarrow}^{\dagger} d_{\mathbf{r}, \downarrow}, \quad (1)$$

where $d_{\mathbf{r}, \sigma}^{\dagger}$ creates an electron with spin σ at site \mathbf{r} , \mathcal{P} projects onto the single- and double-occupied states at each site, and $\hat{\sigma}_{\mathbf{r}}^{\alpha} = \sum_{i,j} d_{\mathbf{r}, i}^{\dagger} \sigma_{ij}^{\alpha} d_{\mathbf{r}, j}$ is the spin operator. We describe the fractionalization of electrons with an $\text{SU}(2)$ parton mean-field theory where each electron operator is decomposed as $d_{\mathbf{r}, \sigma}^{\dagger} = \frac{1}{\sqrt{2}}(a_{\mathbf{r}, 1}^{\dagger} f_{\mathbf{r}, \sigma}^{\dagger} - \eta a_{\mathbf{r}, 2}^{\dagger} f_{\mathbf{r}, \bar{\sigma}}^{\dagger})$ with $\eta = \pm 1$ and $\bar{\sigma} = \downarrow, \uparrow$ for $\sigma = \uparrow, \downarrow$, respectively [53]. The bosonic chargons $a_{\mathbf{r}, \mu}^{\dagger}$ carry the charge of the electron, while the fermionic spinons $f_{\mathbf{r}, \sigma}^{\dagger}$ carry its spin. We assume for concreteness that the Kitaev interaction is ferromagnetic ($K > 0$) and that the electron hopping $\propto t$ is spin-independent. We emphasize, however, that our key results do not depend on these assumptions and should apply whenever electron fractionalization takes place.

To find a quadratic problem for the partons $a_{\mathbf{r}, \mu}$ and $f_{\mathbf{r}, \sigma}$, we use a mean-field decoupling of the hopping term

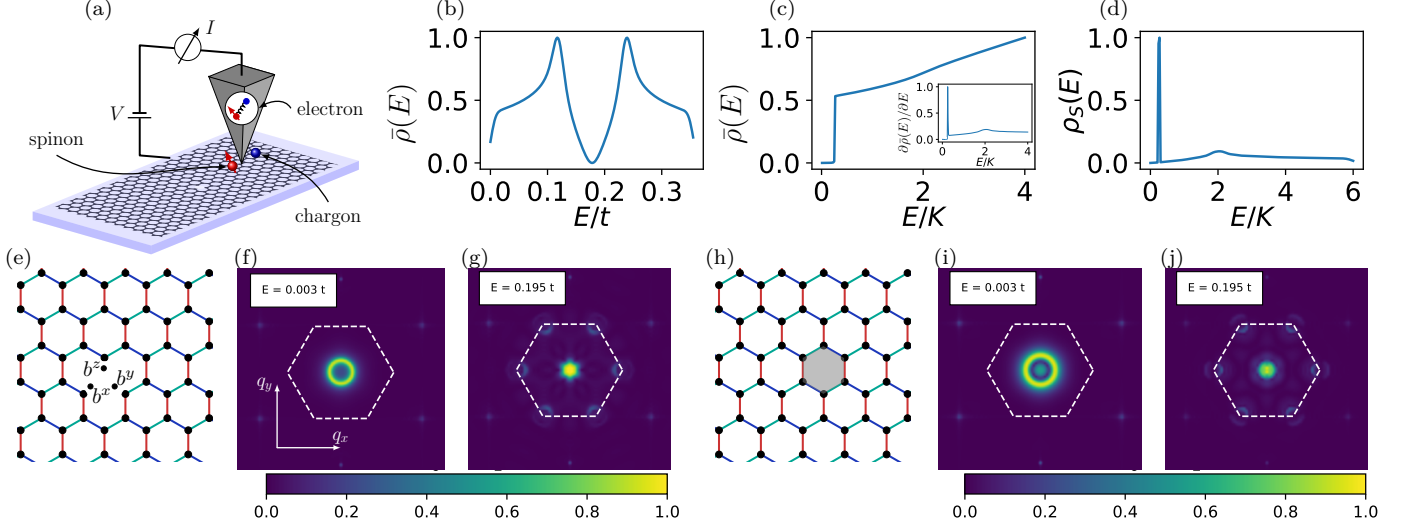


FIG. 1. (a) Schematic view of an STM experiment performed on a Kitaev QSL. An electron leaving the STM tip is fractionalized into a bosonic chargon carrying the charge and a fermionic spinon carrying the spin. (b-d) STM response of a clean system for fast hopping ($t = 10^3 K$). (b) Electron DOS at high energies, i.e., well above the Mott gap, follows the chargon DOS showing a graphene-like DOS. (c) Electron DOS (main plot) and its derivative (inset) at low energies, i.e., just above the Mott gap. In this regime, the derivative of the electron DOS follows the spinon DOS. (d) Spinon DOS with a graphene-like component from matter fermions and a sharp peak due to vison pairs. Note that the sharp peak in the spinon DOS corresponds to a step feature in the electron DOS. (e-j) QPI in the STM response around (e-g) a spin vacancy and (h-j) a localized vison for fast hopping ($t = 10^3 K$). (e,h) Schematic picture of the given defect. (f,g,i,j) Momentum-space electron LDOS around the given defect inside the chargon band where the chargons have (f,i) quadratic and (g,j) Dirac-like dispersion. The white dotted line indicates the first Brillouin zone. In (b) and (c), the electron LDOS is normalized $\bar{\rho} \equiv (\rho - \rho_{\min})/(\rho_{\max} - \rho_{\min})$.

in Eq. (1). The resulting mean-field Hamiltonian is found in the Supplemental Material (SM) [56] to be

$$H_{\text{MF}} = K \sum_{\langle \mathbf{r}, \mathbf{r}' \rangle_{\alpha}} u_{\mathbf{r}, \mathbf{r}'}^{\alpha} c_{\mathbf{r}} c_{\mathbf{r}'} + \frac{t}{8} \sum_{\langle \mathbf{r}, \mathbf{r}' \rangle} \sum_{\mu} i W_{\mathbf{r}, \mathbf{r}'} a_{\mathbf{r}, \mu}^{\dagger} a_{\mathbf{r}', \mu} + \tilde{U} \sum_{\mathbf{r}, \mu} a_{\mathbf{r}, \mu}^{\dagger} a_{\mathbf{r}, \mu}, \quad (2)$$

where the spinons are expressed in the Majorana representation as $f_{\mathbf{r}, \uparrow} = \frac{1}{2}(c_{\mathbf{r}} + ib_{\mathbf{r}}^z)$ and $f_{\mathbf{r}, \downarrow} = \frac{1}{2}(ib_{\mathbf{r}}^x + b_{\mathbf{r}}^y)$ with the matter fermions $c_{\mathbf{r}}$ and the associated Z_2 gauge fields $u_{\mathbf{r}, \mathbf{r}'}^{\alpha} = ib_{\mathbf{r}, \mathbf{r}'}^{\alpha} = \pm 1$ on the $\alpha = x, y, z$ bonds, as well as the mean-field parameters $W_{\mathbf{r}, \mathbf{r}'}$ [53]. In a clean system without any defects, $W_{\mathbf{r}, \mathbf{r}'} \approx 0.475$ for all bonds, and the chargons thus have an effective hopping strength of $tW_{\mathbf{r}, \mathbf{r}'}/8 \approx 0.059t$. The chargon dispersion is then the standard graphene dispersion shifted by energy \tilde{U} , with a bandwidth $\Lambda_C = 3tW_{\mathbf{r}, \mathbf{r}'}/4 \approx 0.356t$ and a Mott gap $U = \tilde{U} - \Lambda_C/2 > 0$. There are also two Dirac points at finite energy \tilde{U} , corresponding to the \mathbf{K} and \mathbf{K}' points of the Brillouin zone (BZ). The matter-fermion dispersion is the standard graphene dispersion with no energy shift, but is only physical at positive energies, and thus extends down to zero energy with a bandwidth $\Lambda_S = 6K$. Finally, flipping a Z_2 gauge field $u_{\mathbf{r}, \mathbf{r}'}^{\alpha}$ from $+1$ to -1 at any given bond creates a pair of localized gauge fluxes (i.e., visons) at the two neighboring hexagons. These vison pairs form a flat band at constant energy $E_V \approx 0.26K$.

An STM experiment measures the differential tunneling conductance, dI/dV , which is proportional to the electron local density of states (LDOS),

$$\rho(\mathbf{r}, E) = \sum_{m, n, \sigma} |\langle \Psi_{mn} | d_{\mathbf{r}, \sigma}^{\dagger} | \Psi_0 \rangle|^2 \delta(E_{mn} - E), \quad (3)$$

where $E = eV - U$ is the bias voltage measured from the Mott gap, and $E_{mn} + U$ is the energy of the excited state $|\Psi_{mn}\rangle$ relative to the ground state $|\Psi_0\rangle$. Each state $|\Psi_0\rangle$ and $|\Psi_{mn}\rangle$ is a product state of a chargon state and a spinon state, $|\Psi_0\rangle = |\Psi_0^C\rangle \otimes |\Psi_0^S\rangle$ and $|\Psi_{mn}\rangle = |\Psi_m^C\rangle \otimes |\Psi_n^S\rangle$, where $|\Psi_0^C\rangle$ is the chargon vacuum and $|\Psi_0^S\rangle$ is the ground state of the first term in Eq. (2). With our definition of E , note that $\rho(\mathbf{r}, E)$ is finite down to $E = 0$ and is zero for $E < 0$. The electron LDOS can then be written as a convolution,

$$\rho(\mathbf{r}, E) = \int_0^E dE' \rho_C(\mathbf{r}, E - E') \rho_S(\mathbf{r}, E'), \quad (4)$$

where $\rho_C(\mathbf{r}, E)$ and $\rho_S(\mathbf{r}, E)$ are the chargon LDOS and spinon LDOS, respectively,

$$\rho_C(\mathbf{r}, E) = \sum_m \sum_{\mu} |\langle \Psi_m^C | a_{\mathbf{r}, \mu}^{\dagger} | \Psi_0^C \rangle|^2 \delta(E_m^C - E), \quad (5)$$

$$\rho_S(\mathbf{r}, E) = \sum_n \left[|\langle \Psi_n^S | c_{\mathbf{r}} | \Psi_0^S \rangle|^2 + \sum_{\alpha} |\langle \Psi_n^S | b_{\mathbf{r}}^{\alpha} | \Psi_0^S \rangle|^2 \right] \delta(E_n^S - E), \quad (6)$$

with $c_{\mathbf{r}}$ creating matter fermions and $b_{\mathbf{r}}^{\alpha}$ exciting pairs of visons. Note that E_m^C has the same shift as E_{mn} such that $\rho_C(\mathbf{r}, E)$ is finite down to $E = 0$.

Results for fast hopping.—We first discuss the conductance spectrum at fast hopping, $t \gg K$, for a clean system with no defects. In a clean system, the differential conductance is identical for all sites, and we can thus drop the site index \mathbf{r} from each density of states (DOS) in Eqs. (4)-(6). According to Eq. (4), the electron DOS $\rho(E)$ is then a convolution of a graphene-like chargon DOS $\rho_C(E)$ and a spinon DOS $\rho_S(E)$ with two components: a graphene-like contribution coming from matter fermions, and a sharp peak at energy $E_V \approx 0.26K$ corresponding to vison pairs. The full range of $\rho(E)$ is plotted in Fig. 1(b); $\rho(E)$ follows $\rho_C(E)$ with bandwidth $\Lambda_C \approx 0.356t$ and a graphene-like structure including a linear node in the center and two Van Hove singularities around it. To understand this result, we first notice that $\Lambda_C \gg \Lambda_S$ for $t \gg K$. Hence, for any $E \gg \Lambda_S$, we can approximate the chargon LDOS with a constant in Eq. (4) (since $E' < \Lambda_S \ll E$) to obtain

$$\rho(\mathbf{r}, E) \approx \rho_C(\mathbf{r}, E) \int_0^{\Lambda_S} dE' \rho_S(\mathbf{r}, E') = 4\rho_C(\mathbf{r}, E), \quad (7)$$

where we use a sum rule for the spinon LDOS in the last step. Therefore, we find $\rho(E) \sim \rho_C(E)$ at $E \gg \Lambda_S$. For $E < \Lambda_S$, in contrast, $\rho(E)$ plotted in Fig. 1(c) exhibits a pronounced step at $E \approx E_V \approx 0.26K$. Furthermore, its derivative, $\partial\rho(E)/\partial E$ [see inset of Fig. 1(c)], appears to follow $\rho_S(E)$ [see Fig. 1(d)] with a sharp peak at $E \approx E_V$ originating from vison pairs and a much broader peak at $E \approx 2K$ corresponding to the matter-fermion Van Hove singularity. To understand this correspondence between $\partial\rho(E)/\partial E$ and $\rho_S(E)$, we differentiate Eq. (4),

$$\begin{aligned} \frac{\partial\rho(\mathbf{r}, E)}{\partial E} &= \rho_C(\mathbf{r}, E=0)\rho_S(\mathbf{r}, E) \\ &+ \int_0^E dE' \frac{\partial\rho_C(\mathbf{r}, E-E')}{\partial E} \rho_S(\mathbf{r}, E'), \end{aligned} \quad (8)$$

and notice that the first term, $O(1/Kt)$, dominates the second term, $O(1/t^2)$, producing the desired result.

We now turn to studying the electron LDOS around a defect. We consider two types of naturally occurring defects: a spin vacancy [see Fig. 1(e)], and a localized vison excitation of the QSL with no accompanying structural defect [see Fig. 1(h)]. Like in the clean system, at high bias voltages, $E \gg \Lambda_S = 6K$, the electron LDOS resembles the chargon LDOS. The momentum-space electron LDOS, $\rho(\mathbf{q}, E) \sim \int d^2\mathbf{r} \rho(\mathbf{r}, E) e^{-i\mathbf{q}\cdot\mathbf{r}}$, is shown around a

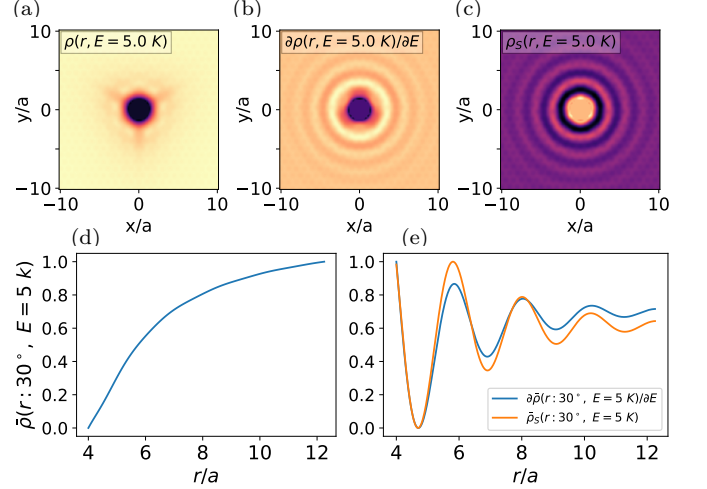


FIG. 2. Low-energy QPI around a spin vacancy for fast hopping ($t = 10^4 K$). (a,b) Electron LDOS (a) and its derivative (b) around the vacancy. (c) Spinon LDOS around the vacancy. (d) Radial line cut for the electron LDOS. (e) Radial line cut for the derivative of the electron LDOS (blue line) and the spinon LDOS (orange line). While the electron LDOS itself looks featureless, its derivative exhibits clear oscillations following the spinon LDOS.

spin vacancy [see Figs. 1(f,g)] and a localized vison [see Figs. 1(i,j)] for two different energies. At the bottom of the chargon band ($E = 0.003t$), the chargon dispersion is quadratic, and the QPI thus exhibits a ring-like feature whose radius is determined by the chargon momentum corresponding to energy E [see Figs. 1(f,i)]. In the middle of the chargon band ($E = 0.195t$), however, the chargons have a Dirac-like dispersion, and the QPI features a filled circle, as opposed to a ring, in the middle of the BZ resulting from the suppressed intra-nodal scattering due to the pseudospin texture [see Figs. 1(g,j)]. There are also arch-looking patterns at the corners of the BZ resulting from the inter-nodal scattering between the \mathbf{K} and \mathbf{K}' Dirac points. We note that analogous features have been discussed for graphene [34, 57]. Interestingly, the QPI is similar for a vacancy and a vison; thus, in the absence of any structural defect, the QPI can serve as evidence of a localized vison, which in turn binds a Majorana zero mode under a magnetic field. It is also worth noting that the effect of a vison is felt by the chargons through renormalized hopping amplitudes of the chargons around the vison. The vison is spatially localized in a hexagon and, therefore, produces a QPI similar to a vacancy.

Next, we consider the more interesting regime of low bias voltages, $E < \Lambda_S = 6K$, where the spinons play an important role in the electron LDOS. In this regime, the electron LDOS is plotted around a vacancy in Fig. 2(a) with a radial line cut shown in Fig. 2(d). While the electron LDOS itself appears featureless, its derivative with respect to energy [see Eq. (8)] exhibits distinctive oscillations, as plotted around a vacancy in Fig. 2(b) with a

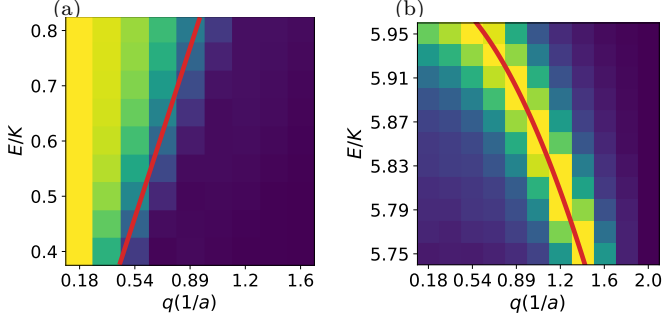


FIG. 3. Extraction of the matter-fermion (i.e., spinon) dispersion for fast hopping ($t = 10^4 K$). The energy derivative of the electron LDOS, $\partial\rho(\mathbf{q}, E)/\partial E$, is plotted against both momentum $q = |\mathbf{q}|$ and energy E inside the spinon band where the spinons have (a) Dirac-like and (b) quadratic dispersion. (a) The Dirac point with velocity v is reflected in a sharp step at $q = 2E/v$. (b) The spinon dispersion $\mathcal{E}(\mathbf{k})$ can be extracted by tracing the sharp peak at $q = 2\mathcal{E}^{-1}(E)$. In each panel, the red line marks the expected position of the appropriate sharp feature (step or peak) from the Kitaev model.

radial line cut shown in Fig. 2(e). Moreover, as observed by comparing Figs. 2(b,e) and Figs. 2(c,e), the derivative of the electron LDOS, $\partial\rho(\mathbf{r}, E)/\partial E$, largely follows the spinon LDOS $\rho_S(\mathbf{r}, E)$. This result is readily explained by Eq. (8) and leads to the remarkable observation that one can directly extract the spinon LDOS from the differential tunneling conductance by taking its derivative with respect to the bias voltage. We further remark that, at very low bias voltages, $E < E_V$, the electron LDOS is mainly contributed from vison pairs near the vacancy, which endows the LDOS with a characteristic three-lobe structure similar to Fig. 4 (b) (Actual results are shown in the SM [56]).

We finally extract the matter-fermion dispersion $\mathcal{E}(\mathbf{k})$ by tracing the spinon LDOS, $\rho_S(\mathbf{r}, E) \sim \partial\rho(\mathbf{r}, E)/\partial E$, in momentum space as the bias voltage E is tuned between $E_V \approx 0.26K$ and $\Lambda_S = 6K$. In Fig. 3(a), $\partial\rho(\mathbf{q}, E)/\partial E$ is plotted against $q = |\mathbf{q}|$ for voltages $E < K$, i.e., close to the Dirac point at the bottom of the matter-fermion band. In this regime, $\partial\rho(\mathbf{q}, E)/\partial E$ exhibits a filled circle at each voltage E [cf. Figs. 1(g,j)] with a sharp step at its radius, $q_{\text{QPI}} = 2E/v$, where v is the matter-fermion velocity at the Dirac point. Hence, this step feature confirms the existence of a matter-fermion Dirac point in the Kitaev QSL. In Fig. 3(b), $\partial\rho(\mathbf{q}, E)/\partial E$ is plotted at the top of the matter-fermion band where the dispersion is quadratic. In this regime, $\partial\rho(\mathbf{q}, E)/\partial E$ possesses a sharp ring-like feature at each voltage E [cf. Figs. 1(f,i)], with its peak radius q_{QPI} being twice the matter-fermion momentum corresponding to energy E . Indeed, the ring-like feature in Fig. 3(b) follows $E = \mathcal{E}(\mathbf{q}/2)$ and can thus be exploited to directly extract the matter-fermion dispersion $\mathcal{E}(\mathbf{k})$ of the Kitaev QSL.

Results for slow hopping.—In the regime of slow hop-

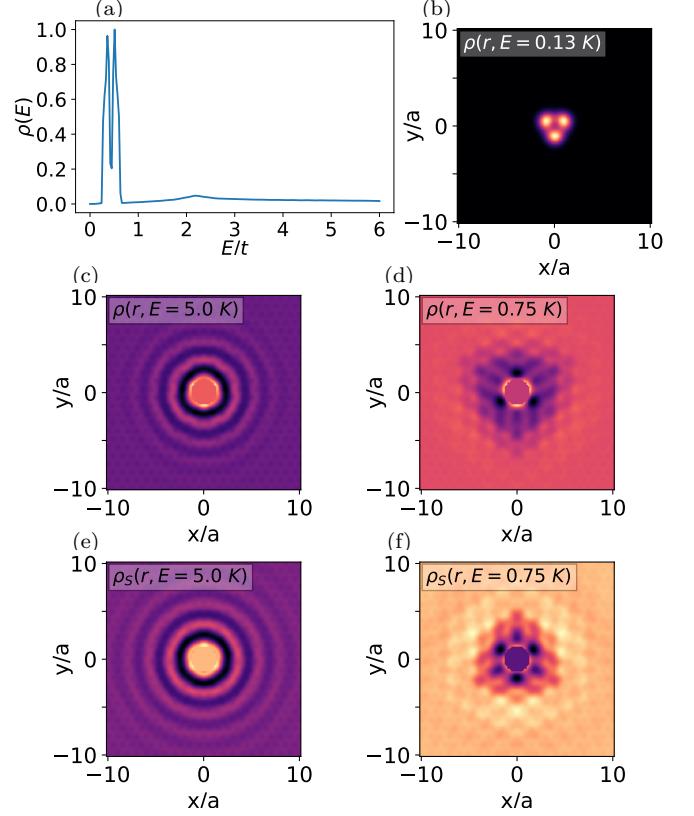


FIG. 4. STM response for slow hopping ($t = K$). (a) Electron DOS for a clean system. (b-f) QPI around a spin vacancy. (b-d) Electron LDOS at $E = 0.13K$, $5K$, and $0.75K$, respectively. (e,f) Spinon LDOS at $E = 5K$ and $0.75K$, respectively.

ping, $t \lesssim K$, the chargon bandwidth is much smaller than the spinon bandwidth, $\Lambda_C \ll \Lambda_S$, because $\Lambda_C \approx 0.356t$ and $\Lambda_S = 6K$. Thus, for any bias voltage $E \gg \Lambda_C$, one may use an approximation analogous to Eq. (7), but with interchanged roles of the spinons and the chargons, to argue that the electron LDOS $\rho(\mathbf{r}, E)$ largely follows the spinon LDOS $\rho_S(\mathbf{r}, E)$. The only caveat is that $\rho_S(\mathbf{r}, E)$ is not smooth at the vison energy, $E_V \approx 0.26K$, which restricts this approximation to $E \gg \max(\Lambda_C, E_V)$. Indeed, while the electron DOS of a clean system shown in Fig. 4(a) resembles the spinon DOS [see Fig. 1(d)] for $E \gtrsim K$, with a broad peak at $E \approx 2K$ due to the matter-fermion Van Hove singularity, the sharp peak at $E \approx E_V$ coming from vison pairs is doubled as it is convolved with the bimodal chargon DOS [see Fig. 1(b)]. In the presence of vacancy, for E near E_V , the contribution to the electron LDOS near a vacancy is dominated by the flat vison bands, which yields well localized three-lobe structure as shown in Fig. 4 (b). When $E \gg \max(\Lambda_C, E_V)$, electron LDOS [Fig. 4(c)] shows clear oscillations following those of the spinon LDOS [Fig. 4(e)]. This result suggests an even more direct correspondence between the QPI and the matter-fermion dispersion than in the pre-

vious regime of fast hopping. For $E \sim \max(\Lambda_C, E_V)$, there is no clear separation of energy scale between chargin and spinon, because the bias voltage is not enough to access the full spinon band. Nevertheless, clear spatial oscillation of electron LDOS occurs [Fig. 4 (d)] although a direct correspondence to the directly calculated spinon LDOS [Fig. 4 (f)] is less obvious.

Conclusions— We study QPI in a Kitaev QSL next to an impurity, as directly measurable in an STM experiment. Employing a parton mean-field theory, we obtain the electron LDOS as a convolution of the chargin and spinon LDOS, and highlight several distinctive features that can help identify the Kitaev QSL. First, we point out that the electron DOS of a clean system exhibits signatures of both vison pairs at $E \approx E_V \approx 0.26K$ and a matter-fermion (i.e., spinon) Van Hove singularity at $E \approx 2K$. Second, in the presence of an impurity, we describe a simple protocol to extract the spinon LDOS and, hence, the spinon dispersion from the measured electron LDOS, thus providing direct evidence of a spinon Dirac point with linear dispersion at low energy. This protocol is remarkable because it allows us to access key spinon properties that are otherwise hard to measure due to the fractionalized nature of the spinons. We also emphasize that the QPI exhibits similar behavior near structural defects like spin vacancies and localized vison excitations that do not alter the structure but act like impurities for spinons. Our results indicate that QPI is a powerful technique for identifying both the Kitaev QSL and its fractionalized excitations. Moreover, our approach readily generalizes to other types of QSLs, such as $U(1)$ QSLs with spinon Dirac points or Fermi surfaces.

Acknowledgments.— We thank Yuji Matsuda, Cristian Batista, and Natalia Perkins for helpful discussions, and particularly Yuji Matsuda for sharing their unpublished manuscript. The work at LANL was carried out under the auspices of the U.S. DOE NNSA under contract No. 89233218CNA000001 through the LDRD Program, and was supported by the Center for Nonlinear Studies at LANL, and was performed, in part, at the Center for Integrated Nanotechnologies, an Office of Science User Facility operated for the U.S. DOE Office of Science, under user proposals #2018BU0010 and #2018BU0083. G.B.H. was supported by the U.S. Department of Energy, Office of Science, National Quantum Information Science Research Centers, Quantum Science Center.

* szl@lanl.gov

- [1] L. Balents, Spin liquids in frustrated magnets, *Nature* **464**, 199 (2010).
- [2] L. Savary and L. Balents, Quantum spin liquids: a review, *Reports on Progress in Physics* **80**, 016502 (2017).
- [3] Y. Zhou, K. Kanoda, and T.-K. Ng, Quantum spin liquid states, *Rev. Mod. Phys.* **89**, 025003 (2017).
- [4] J. Knolle and R. Moessner, A field guide to spin liquids, *Annual Review of Condensed Matter Physics* **10**, 451 (2019).
- [5] C. Broholm, R. J. Cava, S. A. Kivelson, D. G. Nocera, M. R. Norman, and T. Senthil, Quantum spin liquids, *Science* **367**, eaay0668 (2020), <https://www.science.org/doi/pdf/10.1126/science.aay0668>.
- [6] P. W. Anderson, The resonating valence bond state in La_2CuO_4 and superconductivity, *Science* **235**, 1196 (1987), <https://www.science.org/doi/pdf/10.1126/science.235.4793.1196>.
- [7] A. Kitaev, Fault-tolerant quantum computation by anyons, *Ann. Phys.* **303**, 2 (2003).
- [8] C. Nayak, S. H. Simon, A. Stern, M. Freedman, and S. Das Sarma, Non-abelian anyons and topological quantum computation, *Rev. Mod. Phys.* **80**, 1083 (2008).
- [9] A. Stern and N. H. Lindner, Topological quantum computation—from basic concepts to first experiments, *Science* **339**, 1179–1184 (2013).
- [10] A. Kitaev, Anyons in an exactly solved model and beyond, *Annals of Physics* **321**, 2 (2006), arXiv:cond-mat/0506438.
- [11] M. Hermanns, I. Kimchi, and J. Knolle, Physics of the kitaev model: Fractionalization, dynamic correlations, and material connections, *Annual Review of Condensed Matter Physics* **9**, 17 (2018).
- [12] Y. Motome and J. Nasu, Hunting majorana fermions in kitaev magnets, *Journal of the Physical Society of Japan* **89**, 012002 (2020), <https://doi.org/10.7566/JPSJ.89.012002>.
- [13] S. Trebst and C. Hickey, Kitaev materials, *Physics Reports* **950**, 1 (2022), kitaev materials.
- [14] G. Jackeli and G. Khaliullin, Mott insulators in the strong spin-orbit coupling limit: From heisenberg to a quantum compass and kitaev models, *Phys. Rev. Lett.* **102**, 017205 (2009).
- [15] Y. Singh and P. Gegenwart, Antiferromagnetic mott insulating state in single crystals of the honeycomb lattice material Na_2IrO_3 , *Phys. Rev. B* **82**, 064412 (2010).
- [16] X. Liu, T. Berlijn, W.-G. Yin, W. Ku, A. Tsvelik, Y.-J. Kim, H. Gretarsson, Y. Singh, P. Gegenwart, and J. P. Hill, Long-range magnetic ordering in Na_2IrO_3 , *Phys. Rev. B* **83**, 220403 (2011).
- [17] Y. Singh, S. Manni, J. Reuther, T. Berlijn, R. Thomale, W. Ku, S. Trebst, and P. Gegenwart, Relevance of the heisenberg-kitaev model for the honeycomb lattice iridates A_2IrO_3 , *Phys. Rev. Lett.* **108**, 127203 (2012).
- [18] S. Hwan Chun, J.-W. Kim, J. Kim, H. Zheng, C. C. Stoumpos, C. D. Malliakas, J. F. Mitchell, K. Mehlawat, Y. Singh, Y. Choi, T. Gog, A. Al-Zein, M. Sala, M. Krisch, J. Chaloupka, G. Jackeli, G. Khaliullin, and B. J. Kim, Direct evidence for dominant bond-directional interactions in a honeycomb lattice iridate Na_2IrO_3 , *Nature Physics* **11**, 462 (2015).
- [19] K. W. Plumb, J. P. Clancy, L. J. Sandilands, V. V. Shankar, Y. F. Hu, K. S. Burch, H.-Y. Kee, and Y.-J. Kim, $\alpha - \text{RuCl}_3$: A spin-orbit assisted mott insulator on a honeycomb lattice, *Phys. Rev. B* **90**, 041112 (2014).
- [20] J. A. Sears, M. Songvilay, K. W. Plumb, J. P. Clancy, Y. Qiu, Y. Zhao, D. Parshall, and Y.-J. Kim, Magnetic order in $\alpha - \text{RuCl}_3$: A honeycomb-lattice quantum magnet with strong spin-orbit coupling, *Phys. Rev. B* **91**, 144420 (2015).
- [21] M. Majumder, M. Schmidt, H. Rosner, A. A. Tsirlin, H. Yasuoka, and M. Baenitz, Anisotropic $\text{Ru}^{3+}4d^5$ mag-

- netism in the α - ruCl_3 honeycomb system: Susceptibility, specific heat, and zero-field nmr, *Phys. Rev. B* **91**, 180401 (2015).
- [22] H.-S. Kim, V. S. V., A. Catuneanu, and H.-Y. Kee, Kitaev magnetism in honeycomb ruCl_3 with intermediate spin-orbit coupling, *Phys. Rev. B* **91**, 241110 (2015).
- [23] H. B. Cao, A. Banerjee, J.-Q. Yan, C. A. Bridges, M. D. Lumsden, D. G. Mandrus, D. A. Tennant, B. C. Chakoumakos, and S. E. Nagler, Low-temperature crystal and magnetic structure of α - ruCl_3 , *Phys. Rev. B* **93**, 134423 (2016).
- [24] Y. Kasahara, T. Ohnishi, Y. Mizukami, O. Tanaka, S. Ma, K. Sugii, N. Kurita, H. Tanaka, J. Nasu, Y. Motome, T. Shibauchi, and Y. Matsuda, Majorana quantization and half-integer thermal quantum hall effect in a kitaev spin liquid, *Nature* **559**, 227–231 (2018).
- [25] M. Yamashita, J. Gouchi, Y. Uwatoko, N. Kurita, and H. Tanaka, Sample dependence of half-integer quantized thermal hall effect in the kitaev spin-liquid candidate α - ruCl_3 , *Phys. Rev. B* **102**, 220404 (2020).
- [26] T. Yokoi, S. Ma, Y. Kasahara, S. Kasahara, T. Shibauchi, N. Kurita, H. Tanaka, J. Nasu, Y. Motome, C. Hickey, S. Trebst, and Y. Matsuda, Half-integer quantized anomalous thermal hall effect in the kitaev material candidate ruCl_3 , *Science* **373**, 568–572 (2021).
- [27] J. A. N. Bruin, R. R. Claus, Y. Matsumoto, N. Kurita, H. Tanaka, and H. Takagi, Robustness of the thermal hall effect close to half-quantization in ruCl_3 , *Nature Physics* **18**, 401–405 (2022).
- [28] L. J. Sandilands, Y. Tian, K. W. Plumb, Y.-J. Kim, and K. S. Burch, Scattering continuum and possible fractionalized excitations in α - ruCl_3 , *Phys. Rev. Lett.* **114**, 147201 (2015).
- [29] J. Nasu, J. Knolle, D. L. Kovrizhin, Y. Motome, and R. Moessner, Fermionic response from fractionalization in an insulating two-dimensional magnet, *Nature Physics* **12**, 912–915 (2016).
- [30] A. Banerjee, C. A. Bridges, J.-Q. Yan, A. A. Aczel, L. Li, M. B. Stone, G. E. Granroth, M. D. Lumsden, Y. Yiu, J. Knolle, S. Bhattacharjee, D. L. Kovrizhin, R. Moessner, D. A. Tennant, D. G. Mandrus, and S. E. Nagler, Proximate kitaev quantum spin liquid behaviour in a honeycomb magnet, *Nature Materials* **15**, 733 (2016).
- [31] A. Banerjee, J. Yan, J. Knolle, C. A. Bridges, M. B. Stone, M. D. Lumsden, D. G. Mandrus, D. A. Tennant, R. Moessner, and S. E. Nagler, Neutron scattering in the proximate quantum spin liquid α - ruCl_3 , *Science* **356**, 1055–1059 (2017).
- [32] S.-H. Do, S.-Y. Park, J. Yoshitake, J. Nasu, Y. Motome, Y. S. Kwon, D. T. Adroja, D. J. Voneshen, K. Kim, T.-H. Jang, J.-H. Park, K.-Y. Choi, and S. Ji, Majorana fermions in the kitaev quantum spin system α - ruCl_3 , *Nature Physics* **13**, 1079–1084 (2017).
- [33] N. Avraham, J. Reiner, A. Kumar-Nayak, N. Morali, R. Batabyal, B. Yan, and H. Beidenkopf, Quasiparticle interference studies of quantum materials, *Advanced Materials* **30**, 10.1002/adma.201707628 (2018).
- [34] C. Bena, Effect of a single localized impurity on the local density of states in monolayer and bilayer graphene, *Physical Review Letters* **100**, 10.1103/physrevlett.100.076601 (2008).
- [35] I. Brihuega, P. Mallet, C. Bena, S. Bose, C. Michaelis, L. Vitali, F. Varchon, L. Magaud, K. Kern, and J. Y. Veuillen, Quasiparticle chirality in epitaxial graphene probed at the nanometer scale, *Phys. Rev. Lett.* **101**, 206802 (2008).
- [36] P. Mallet, I. Brihuega, S. Bose, M. M. Ugeda, J. M. Gómez-Rodríguez, K. Kern, and J. Y. Veuillen, Role of pseudospin in quasiparticle interferences in epitaxial graphene probed by high-resolution scanning tunneling microscopy, *Phys. Rev. B* **86**, 045444 (2012).
- [37] D. Dombrowski, W. Jolie, M. Petrović, S. Runte, F. Craes, J. Klinkhammer, M. Kralj, P. Lazić, E. Sela, and C. Busse, Energy-dependent chirality effects in quasifree-standing graphene, *Phys. Rev. Lett.* **118**, 116401 (2017).
- [38] W.-Y. He and P. A. Lee, Magnetic impurity as a local probe of the $u(1)$ quantum spin liquid with spinon fermi surface, *Phys. Rev. B* **105**, 195156 (2022).
- [39] W. Ruan, Y. Chen, S. Tang, J. Hwang, H.-Z. Tsai, R. L. Lee, M. Wu, H. Ryu, S. Kahn, F. Liou, C. Jia, A. Aikawa, C. Hwang, F. Wang, Y. Choi, S. G. Louie, P. A. Lee, Z.-X. Shen, S.-K. Mo, and M. F. Crommie, Evidence for quantum spin liquid behaviour in single-layer 1t-tase2 from scanning tunnelling microscopy, *Nature Physics* **17**, 1154–1161 (2021).
- [40] Y. Chen, W.-Y. He, W. Ruan, J. Hwang, S. Tang, R. L. Lee, M. Wu, T. Zhu, C. Zhang, H. Ryu, F. Wang, S. G. Louie, Z.-X. Shen, S.-K. Mo, P. A. Lee, and M. F. Crommie, Evidence for a spinon kondo effect in cobalt atoms on single-layer 1t-tase2, *Nature Physics* **18**, 1335–1340 (2022).
- [41] A. Kolezhuk, S. Sachdev, R. R. Biswas, and P. Chen, Theory of quantum impurities in spin liquids, *Phys. Rev. B* **74**, 165114 (2006).
- [42] G. Khaliullin, S. Krivenko, R. Kilian, and P. Fulde, Impurity effects in spin liquids, **282–287**, 1749–1750 (1997).
- [43] K. P. Wójcik and J. Kroha, Quantum spin liquid in an rkky-coupled two-impurity kondo system, *Physical Review B* **107**, 10.1103/physrevb.107.112111 (2023).
- [44] Y. Kohsaka, S. Akutagawa, S. Omachi, Y. Iwamichi, T. Ono, I. Tanaka, S. Tateishi, H. Murayama, S. Suet-sugu, K. Hashimoto, T. Shibauchi, M. O. Takahashi, M. G. Yamada, S. Nikolaev, T. Mizushima, S. Fujimoto, T. Terashima, T. Asaba, Y. Kasahara, and Y. Matsuda, Imaging quantum interference in a monolayer kitaev quantum spin liquid candidate (2024), [arXiv:2403.16553](https://arxiv.org/abs/2403.16553) [cond-mat.str-el].
- [45] X. Zheng, Z. Liu, C. Zhang, H. Zhou, C. Yang, Y. Shi, K. Tanigaki, and R.-R. Du, Observation of unconventional charge order during the transition from mott-insulator to charge-transfer-insulator in α - ruCl_3 (2024), [arXiv:2403.11232](https://arxiv.org/abs/2403.11232) [cond-mat.str-el].
- [46] J. Feldmeier, W. Natori, M. Knap, and J. Knolle, Local probes for charge-neutral edge states in two-dimensional quantum magnets, *Phys. Rev. B* **102**, 134423 (2020).
- [47] E. J. König, M. T. Randeria, and B. Jäck, Tunneling spectroscopy of quantum spin liquids, *Phys. Rev. Lett.* **125**, 267206 (2020).
- [48] T. Bauer, L. R. D. Freitas, R. G. Pereira, and R. Egger, Scanning tunneling spectroscopy of majorana zero modes in a kitaev spin liquid, *Phys. Rev. B* **107**, 054432 (2023).
- [49] M. O. Takahashi, M. G. Yamada, M. Udagawa, T. Mizushima, and S. Fujimoto, Nonlocal spin correlation as a signature of ising anyons trapped in vacancies of the kitaev spin liquid, *Phys. Rev. Lett.* **131**, 236701 (2023).
- [50] W.-H. Kao, N. B. Perkins, and G. B. Halász, Vacancy

- spectroscopy of non-abelian kitaev spin liquids, [Phys. Rev. Lett. **132**, 136503 \(2024\)](#).
- [51] W.-H. Kao, G. B. Halász, and N. B. Perkins, Dynamics of vacancy-induced modes in the non-abelian kitaev spin liquid, [Phys. Rev. B **109**, 125150 \(2024\)](#).
 - [52] T. Bauer, L. R. D. Freitas, E. Andrade, R. Egger, and R. G. Pereira, [Scanning tunneling spectroscopy of magnetic quantum impurities in two-dimensional magnets \(2024\)](#), [arXiv:2405.19962 \[cond-mat.str-el\]](#).
 - [53] Y.-Z. You, I. Kimchi, and A. Vishwanath, Doping a spin-orbit mott insulator: Topological superconductivity from the kitaev-heisenberg model and possible application to $(\text{Na}_2/\text{Li}_2)\text{FeO}_3$, [Phys. Rev. B **86**, 085145 \(2012\)](#).
 - [54] W. Kadow, H.-K. Jin, J. Knolle, and M. Knap, Single-hole spectra of kitaev spin liquids: from dynamical nagaoka ferromagnetism to spin-hole fractionalization, [npj Quantum Materials **9**, 10.1038/s41535-024-00641-7 \(2024\)](#).
 - [55] H.-K. Jin, W. Kadow, M. Knap, and J. Knolle, Kinetic ferromagnetism and topological magnons of the hole-doped kitaev spin liquid (2023), [arXiv:2309.15153 \[cond-mat.str-el\]](#).
 - [56] See supplementary materials.
 - [57] C. Bena, Green's functions and impurity scattering in graphene, [Phys. Rev. B **79**, 125427 \(2009\)](#).
 - [58] G. F. Bertsch and L. M. Robledo, Symmetry restoration in hartree-fock-bogoliubov based theories, [Phys. Rev. Lett. **108**, 042505 \(2012\)](#).
 - [59] B. G. Carlsson and J. Rotureau, New and practical formulation for overlaps of bogoliubov vacua, [Phys. Rev. Lett. **126**, 172501 \(2021\)](#).

Supplementary materials for “theory of quasiparticle interference in Kitaev quantum spin liquids”

Ammar Jahin,¹ Hao Zhang,^{1,2} Gábor B. Halász,^{3,4} and Shi-Zeng Lin^{1,2,5,*}

¹Theoretical Divison, T-4, Los Alamos National Laboratory, Los Alamos, New Mexico 87545, USA

²CLNS, Los Alamos National Laboratory, Los Alamos, New Mexico 87545, USA

³Materials Science and Technology Divison, Oak Ridge National Laboratory, Oak Ridge, Tennessee 37831, USA

⁴Quantum Science Center, Oak Ridge, Tennessee 37831, USA

⁵Center for Integrated Nanotechnologies (CINT),

Los Alamos National Laboratory, Los Alamos, New Mexico 87545, USA

(Dated: July 8, 2024)

Parton decomposition and evaluation of the mean-field parameters

In this section, we give the details for the parton construction and the mean-field theory Hamiltonian we use in the main text. The Hamiltonian governing the electron hopping is,

$$H_t = -t \sum_{\langle \mathbf{r}, \mathbf{r}' \rangle} \sum_{\sigma} [\mathcal{P} d_{\mathbf{r}, \sigma}^{\dagger} d_{\mathbf{r}', \sigma} \mathcal{P} + \text{h.c.}] . \quad (1)$$

where \mathcal{P} projects out the local empty states. We express the local electronic degrees of freedom in terms of two flavors of chargons $a_{\mathbf{r}, \mu}$ and two flavors of spinons $f_{\mathbf{r}, \sigma}$

$$d_{\mathbf{r}, \uparrow}^{\dagger} = \frac{1}{\sqrt{2}} (a_{\mathbf{r}, 1}^{\dagger} f_{\mathbf{r}, \uparrow}^{\dagger} - a_{\mathbf{r}, 2}^{\dagger} f_{\mathbf{r}, \downarrow}^{\dagger}) \quad d_{\mathbf{r}, \downarrow}^{\dagger} = \frac{1}{\sqrt{2}} (a_{\mathbf{r}, 1}^{\dagger} f_{\mathbf{r}, \downarrow}^{\dagger} + a_{\mathbf{r}, 2}^{\dagger} f_{\mathbf{r}, \uparrow}^{\dagger}), \quad (2)$$

Such construction introduces an SU(2) gauge freedom, which is best seen rewriting the above equations as,

$$\mathcal{D}_{\mathbf{r}} = \frac{1}{\sqrt{2}} \mathcal{F}_{\mathbf{r}} \mathcal{A}_{\mathbf{r}} \quad (3)$$

with,

$$\mathcal{D}_{\mathbf{r}} = \begin{bmatrix} d_{\mathbf{r}, \uparrow}^{\dagger} & -d_{\mathbf{r}, \downarrow}^{\dagger} \\ d_{\mathbf{r}, \downarrow}^{\dagger} & d_{\mathbf{r}, \uparrow}^{\dagger} \end{bmatrix}, \quad \mathcal{F} = \begin{bmatrix} f_{\mathbf{r}, \uparrow}^{\dagger} & -f_{\mathbf{r}, \downarrow}^{\dagger} \\ f_{\mathbf{r}, \downarrow}^{\dagger} & f_{\mathbf{r}, \uparrow}^{\dagger} \end{bmatrix}, \quad \mathcal{A} = \begin{bmatrix} a_{\mathbf{r}, 1}^{\dagger} & -a_{\mathbf{r}, 2}^{\dagger} \\ a_{\mathbf{r}, 2}^{\dagger} & a_{\mathbf{r}, 1}^{\dagger} \end{bmatrix}. \quad (4)$$

In this form the spin SU(2) rotations are implemented by $\mathcal{D}_{\mathbf{r}} \rightarrow U_s \mathcal{D}_{\mathbf{r}}$. In addition, this expansion of the Hilbert space introduces a gauge freedom in that the physical degrees of freedom $\mathcal{D}_{\mathbf{r}}$ do not change under $\mathcal{F}_{\mathbf{r}} \rightarrow \mathcal{F}_{\mathbf{r}} U_g$ and, $\mathcal{A}_{\mathbf{r}} \rightarrow U_g^{\dagger} \mathcal{A}_{\mathbf{r}}$. The generators of this SU(2) gauge symmetry are,

$$K_{\mathbf{r}}^{\alpha} = \frac{1}{4} \text{Tr} \mathcal{F}_{\mathbf{r}} \sigma^{\alpha} F_{\mathbf{r}}^{\dagger} - \frac{1}{4} \text{Tr} \sigma^z \mathcal{A}_{\mathbf{r}}^{\dagger} \sigma^{\alpha} \mathcal{A}_{\mathbf{r}} \quad (5)$$

The physical Hilbert space is invariant under such gauge transformation, i.e. $K_{\mathbf{r}}^{\alpha} = 0$. It can be shown that only three states satisfy this condition,

$$d_{\mathbf{r}, \uparrow}^{\dagger} |0\rangle = f_{\mathbf{r}, \uparrow}^{\dagger} |\tilde{0}\rangle, \quad d_{\mathbf{r}, \downarrow}^{\dagger} |0\rangle = f_{\mathbf{r}, \downarrow}^{\dagger} |\tilde{0}\rangle, \quad d_{\mathbf{r}, \downarrow}^{\dagger} d_{\mathbf{r}, \uparrow}^{\dagger} |0\rangle = \frac{1}{\sqrt{2}} (a_{\mathbf{r}, 2}^{\dagger} + a_{\mathbf{r}, 1}^{\dagger} f_{\mathbf{r}, \downarrow}^{\dagger} f_{\mathbf{r}, \uparrow}^{\dagger}) |\tilde{0}\rangle. \quad (6)$$

where $d_{\mathbf{r}, \sigma} |0\rangle = 0$ and $f_{\mathbf{r}, \mu} |\tilde{0}\rangle = a_{\mathbf{r}, \mu} |\tilde{0}\rangle = 0$. We choose the decomposition of the electronic degrees of freedom into spinons and chargon so that the physical space coincides with the low energy subspace formed by the single, and doubly occupied local states in the presence of electron doping.

Substituting Eq. 2 in H_t we get,

$$H_t = -t \sum_{\langle \mathbf{r}, \mathbf{r}' \rangle} \left[a_{\mathbf{r}, 1}^{\dagger} a_{\mathbf{r}', 1} \left(f_{\mathbf{r}, \uparrow}^{\dagger} f_{\mathbf{r}', \uparrow}^{\dagger} + f_{\mathbf{r}, \downarrow}^{\dagger} f_{\mathbf{r}', \downarrow}^{\dagger} \right) + a_{\mathbf{r}, 2}^{\dagger} a_{\mathbf{r}', 2} \left(f_{\mathbf{r}, \uparrow}^{\dagger} f_{\mathbf{r}', \uparrow}^{\dagger} + f_{\mathbf{r}, \downarrow}^{\dagger} f_{\mathbf{r}', \downarrow}^{\dagger} \right) \right. \\ \left. + a_{\mathbf{r}, 1}^{\dagger} a_{\mathbf{r}', 2} \left(f_{\mathbf{r}, \downarrow}^{\dagger} f_{\mathbf{r}', \uparrow}^{\dagger} - f_{\mathbf{r}, \uparrow}^{\dagger} f_{\mathbf{r}', \downarrow}^{\dagger} \right) + a_{\mathbf{r}, 2}^{\dagger} a_{\mathbf{r}', 1} \left(f_{\mathbf{r}, \uparrow}^{\dagger} f_{\mathbf{r}', \downarrow}^{\dagger} - f_{\mathbf{r}, \downarrow}^{\dagger} f_{\mathbf{r}', \uparrow}^{\dagger} \right) + \text{h.c.} \right]. \quad (7)$$

We use a mean-field theory to study this Hamiltonian. We consider the fractionalization region, and the mean-field order parameters for the f bilinears are those of the Kitaev quantum spin liquid. The ansatz takes the following form,

$$H_t^{\text{MF}} = \frac{t}{8} \sum_{\mathbf{r}, \mathbf{r}'} \sum_{\mu} i W_{\mathbf{r}, \mathbf{r}'} a_{\mathbf{r}, \mu}^{\dagger} a_{\mathbf{r}', \mu} \quad (8)$$

where

$$\langle a_{\mathbf{r}, \mu}^{\dagger} a_{\mathbf{r}', \mu'} \rangle = \langle f_{\mathbf{r}, \uparrow}^{\dagger} f_{\mathbf{r}', \downarrow}^{\dagger} \rangle = 0 \quad (9)$$

and

$$W_{\mathbf{r}, \mathbf{r}'} = \langle i c_{\mathbf{r}} c_{\mathbf{r}'} + \sum_{\alpha} i b_{\mathbf{r}}^{\alpha} b_{\mathbf{r}'}^{\alpha} \rangle, \quad (10)$$

where we have defined the Majorana operators,

$$f_{\mathbf{r}, \uparrow}^{\dagger} = \frac{1}{\sqrt{2}}(c_{\mathbf{r}} + i b_{\mathbf{r}}^z), \quad f_{\mathbf{r}, \downarrow}^{\dagger} = \frac{1}{\sqrt{2}}(i b_{\mathbf{r}}^x + b_{\mathbf{r}}^y). \quad (11)$$

The expectation values $W_{\mathbf{r}, \mathbf{r}'}$ are evaluated for the ground state of the Kitaev model with a defect introduced. This requires solving the quadratic Hamiltonian of the Kitaev model which can be done numerically.

The terms $\langle i b_{\mathbf{r}}^{\alpha} b_{\mathbf{r}'}^{\alpha} \rangle$ are easy to compute. They are nonzero only when the product $b_{\mathbf{r}}^{\alpha} b_{\mathbf{r}'}^{\alpha}$ does not create any visons. This happens when \mathbf{r} and \mathbf{r}' are nearest neighbors and make an α -edge,

$$\langle i b_{\mathbf{r}}^{\alpha} b_{\mathbf{r}'}^{\alpha} \rangle = \begin{cases} u_{\mathbf{r}, \mathbf{r}'}^{\text{std}} & \mathbf{r} \text{ and } \mathbf{r}' \text{ make an } \alpha\text{-edge} \\ 0 & \text{otherwise} \end{cases} \quad (12)$$

where $u_{\mathbf{r}, \mathbf{r}'}^{\text{std}}$ is the standard gauge field defining the vison-free subspace away from a defect and zero for edges connected to a vacancy.

The evaluation of $\langle i c_{\mathbf{r}} c_{\mathbf{r}'} \rangle$ requires the diagonalization of the Kitaev Hamiltonian which takes the general form

$$H_K = \frac{K}{2} \sum_{\mathbf{r}, \mathbf{r}'} A_{\mathbf{r}, \mathbf{r}'} i c_{\mathbf{r}} c_{\mathbf{r}'} \quad (13)$$

Since $A_{\mathbf{r}, \mathbf{r}'}$ is an antisymmetric matrix, there exists a matrix $Q \in O(N)$, with N being the number of sites of the system, such that

$$A = Q \mathcal{E} Q^T \quad (14)$$

with

$$\mathcal{E} = \bigoplus_{m=1}^{N/2} \begin{bmatrix} 0 & \varepsilon_m \\ -\varepsilon_m & 0 \end{bmatrix}, \quad \varepsilon_m > 0. \quad (15)$$

Using this to rewrite the Kitaev Hamiltonian, we have

$$H_K = \sum_{m=1}^{N/2} \varepsilon_m i b_{2m} b_{2m+1} = \sum_m \varepsilon_m [2 \psi_m^{\dagger} \psi_m - 1] \quad (16)$$

where we define $b_i = c_{\mathbf{r}} Q_{\mathbf{r}, i}$, and $\psi_m = (b_{2m} + i b_{2m+1})/2$. We obtain the matrix Q numerically which has a computational cost of $O(N^3)$, the same as the exact diagonalization. The ground state of the Kitaev model is defined such that $\psi_m |\Psi_0^S\rangle = 0$ for all m . In the new basis, we can easily evaluate,

$$\langle i b_{2m} b_{2n} \rangle = \langle i b_{2m+1} b_{2n+1} \rangle = i \delta_{m, n}, \quad \langle i b_{2m} b_{2n+1} \rangle = -\delta_{m, n} \quad (17)$$

Using this we can write

$$\langle i c_i c_j \rangle = Q_{j, j'} Q_{i, i'} \langle i b_{i'} b_{j'} \rangle \quad (18)$$

which we evaluate it numerically.

Evaluation of the LDOS

Chargon LDOS

In the main text, we arrive at the following expression for chargon LDOS,

$$\rho_C(\mathbf{r}, E) = \sum_m \sum_\mu |\langle \Psi_m^C | a_{\mathbf{r},\mu}^\dagger | \Psi_0^C \rangle|^2 \delta(E_m^C - E). \quad (19)$$

The excited states $|\Psi_m^C\rangle$ are those of H_t , and are written as,

$$|\Psi_m^C\rangle = a_m^\dagger |\Psi_0^C\rangle, \quad (20)$$

where

$$a_m^\dagger = U_{\mathbf{r},m} a_{\mathbf{r}}^\dagger. \quad (21)$$

We drop the μ index for now, as different species of chargons do not mix. With the matrix elements $W_{\mathbf{r},\mathbf{r}'}$ evaluated, we can numerically calculate $U_{\mathbf{r},m}$ by exactly diagonalizing the Hamiltonian. After obtaining $U_{\mathbf{r},m}$ the chargon LDOS takes the following expression,

$$\rho_C(\mathbf{r}, E) = 2 \sum_m |U_{\mathbf{r},m}|^2 \delta(E_m^C - E), \quad (22)$$

with the factor of 2 from the sum over μ . In numerically evaluating this formula on a finite system size of linear size L the energy level spacing goes to zero as $1/L$.

In all of our numerical computations, we use the Gaussian broadening

$$\delta(E_m^C - E) \approx \frac{1}{\sqrt{2\pi}\sigma^2} \exp\left[-\frac{(E_m^C - E)^2}{2\sigma^2}\right]. \quad (23)$$

This is similar to adding a non-zero inverse lifetime to the quasiparticles. The standard deviation σ is chosen to be of the order of the level spacing and such that the DOS is smooth.

Spinon LDOS

In the main text, we arrive at the following expression for spinon LDOS,

$$\rho_S(\mathbf{r}, E) = \sum_n \left[|\langle \Psi_n^S | c_{\mathbf{r}} | \Psi_0^S \rangle|^2 + \sum_\alpha |\langle \Psi_n^S | b_{\mathbf{r}}^\alpha | \Psi_0^S \rangle|^2 \right] \delta(E_n^S - E). \quad (24)$$

The operator $c_{\mathbf{r}}$ does not change the vison configuration of $|\Psi_0^S\rangle$, and the evaluation of these terms requires only knowing the matrix Q in Eq. (14). From Eq. (16) we see that the excited states contributing to a nonzero overlap of $\langle \Psi_n^S | c_{\mathbf{r}} | \Psi_0^S \rangle$ take the form

$$|\Psi_n^S\rangle = \psi_n^\dagger |\Psi_0^S\rangle, \quad (25)$$

where Ψ_0^S is defined as the state belonging to the vison-free subspace and the vacuum of ψ_m . We write $c_{\mathbf{r}} = Q_{\mathbf{r},i} b_i = Q_{\mathbf{r},2n} b_{2n} + Q_{\mathbf{r},2n+1} b_{2n+1}$, and thus,

$$\langle \Psi_n^S | c_{\mathbf{r}} | \Psi_0^S \rangle = Q_{\mathbf{r},2n} - \frac{1}{i} Q_{\mathbf{r},2n+1} \rightarrow |\langle \Psi_n^S | c_{\mathbf{r}} | \Psi_0^S \rangle|^2 = Q_{\mathbf{r},2n}^2 + Q_{\mathbf{r},2n+1}^2. \quad (26)$$

The evaluation of the overlap $\langle \Psi_n^S | b_{\mathbf{r}}^\alpha | \Psi_0^S \rangle$ is more involved since the operator $b_{\mathbf{r}}^\alpha$ excites two neighboring visons at the plaquettes sharing the α -edge connected to the site \mathbf{r} . The full ground state of the Kitaev model takes a tensor product form,

$$|\Psi_0^S\rangle = |W_0\rangle \otimes |\Phi_0\rangle \quad (27)$$

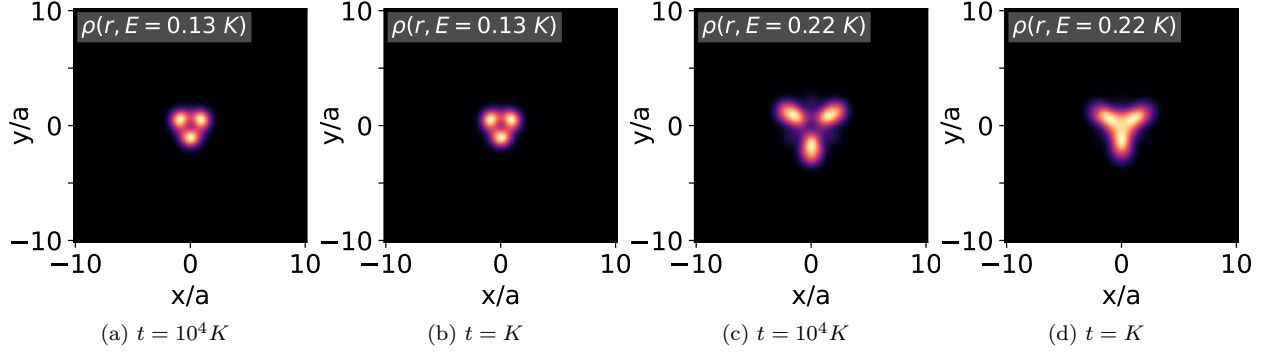


FIG. 1. Electron LDOS near a defect at energies below the energy for exciting a pair of visons $E_V = 0.27K$ in a clean system. We plot electron LDOS for (a) $E = 0.13K$ and $t = 10^4 K$, (b) $E = 0.13K$ and $t = K$, (c) $E = 0.22K$ and $t = 10^4 K$, and (d) $E = 0.22K$ and $t = K$ (d). All plots show that the majority of the weight is near the defect as a result of the flat vison band.

where $|W_0\rangle$ describes the vison configuration, and $|\Phi_0\rangle$ describes the matter fermion c_r as discussed above. The b_r^α operator acts on the vison subspace,

$$b_r^\alpha |\Psi_0^S\rangle = |W'\rangle \otimes |\Phi_0\rangle \quad (28)$$

with $|W'\rangle$ describing the state with two visons excited. To obtain a nonzero overlap $\langle \Psi_n^S | b_r^\alpha | \Psi_0^S \rangle$, the state $|\Psi_n^S\rangle$ must have the same vison configuration as $|b_r^\alpha | \Psi_0^S \rangle$. We can always choose an excited state with a matching vison configuration, so we write

$$|\Psi_n^S\rangle = |W'\rangle \otimes |\Phi'_n\rangle. \quad (29)$$

and obtain

$$\langle \Psi_n^S | b_r^\alpha | \Psi_0^S \rangle = \langle \Phi'_n | \Phi_0 \rangle. \quad (30)$$

There are multiple possibilities for the state $|\Phi'_n\rangle$, the one with the lowest energy being the ground state in the subspace of the excited visons. We label this state as $|\Phi'_0\rangle$ and focus now on the evaluation of $\langle \Phi'_0 | \Phi_0 \rangle$. Similar to how the state $|\Phi_0\rangle$ is defined as the state annihilated by ψ_m , the state $|\Phi'_0\rangle$ is defined as the state annihilated by a different set of operators ψ'_m . Thus, we are asking about the overlap between two different Bogoliubov vacua. This is the same as asking about the overlap between two superconducting states. This overlap is given using what is known in the nuclear physics literature as the “Onishi” formula. We use a more practical formula developed in Ref. [58] which gives the overlap in terms of the Pfaffian,

$$\langle \Phi'_0 | \Phi_0 \rangle = \frac{e^{i\theta}}{\prod_n v'_n \prod_m v_m} \text{Pf} \begin{bmatrix} V^T U & V^T V'^* \\ -V'^\dagger V & U'^T V'^* \end{bmatrix} \quad (31)$$

where

$$\begin{bmatrix} g \\ g^\dagger \end{bmatrix} = \begin{bmatrix} U & V^* \\ V & U^* \end{bmatrix} \begin{bmatrix} \psi \\ \psi^\dagger \end{bmatrix}, \quad g_m = \frac{1}{2}(c_{2i} + c_{2i+1}) \quad (32)$$

and v_m are the singular values of V . The matrices U' , and V' are defined similarly for ψ'_m .

The Pfaffian formula above is numerically challenging to compute when either V or V' has zero singular values. To circumvent this issue, we use the development in Ref. [59] in which we remove the zero singular values using a Bloch-Messiah decomposition of the matrices U and V , and U' and V' . We do not spend effort extracting the exact phase $e^{i\theta}$ since for our problem we are only interested in the magnitude of the overlap.

In principle, the computation might produce $|\Phi_0\rangle$ and $|\Phi'_0\rangle$ that have different fermion parity, leading to a zero overlap. This can always be remedied for in the case of a vacancy where the model contains dangling b^α Majorana operators around the vacancy. These can be combined into a complex fermion that is completely decoupled from the system, and we are free to choose its filling to make the parity of $|\Phi_0\rangle$ and $|\Phi'_0\rangle$ match.

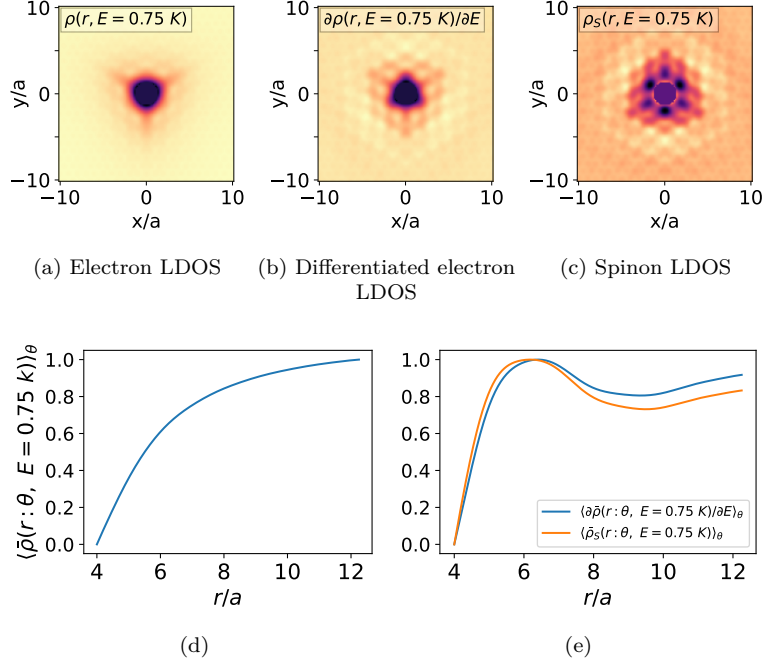


FIG. 2. Results for QPI near the spinon Dirac point at $t = 10^4 K$. The electron LDOS looks featureless away from the defect (a), and (d). However, as shown in (b), taking a derivative with respect to energy reveals the QPI of the spinon. As comparison, the spinon LDOS obtained directly from the model [Eq. (6) in the main text] is displayed in (c). Panel (e) shows a line cut of derivative of the electron LDOS and the spinon LDOS obtained directly from the model on the same plot for comparison.

Every evaluation of the Pfaffian formula incurs a computational cost that is $O(N^3)$ as we solve for U' and V' . In our problem, we need to evaluate this Pfaffian $O(N)$ times corresponding to different locations of the vison excitations on the lattice. In total, the computational cost of evaluating the overlaps $\langle \Phi'_0 | \Phi_0 \rangle$ for all possible excitations is $O(N^4)$. Our calculations show that $|\langle \Phi'_0 | \Phi_0 \rangle|^2 \approx 0.77$ for the two neighboring visons excited by b_r^α .

The next task is to compute the overlap for $|\Phi'_n\rangle$ which represents Bogoliubov quasiparticles excited on top of the vacuum $|\Phi'_0\rangle$. These Bogoliubov excitations must come in pairs to preserve the fermion parity to have a nonzero overlap. In general, this can be done by writing $|\Phi'_n\rangle$ to be the vacuum of $\psi_0'^\dagger, \psi_1'^\dagger, \psi_3, \psi_4, \dots$ where $\psi_0'^\dagger, \psi_1'^\dagger$ are the two excited Bogoliubov quasiparticles. The computational cost of doing this evaluation is $O(N^6)$; $O(N^3)$ for evaluation of the Pfaffian, $O(N)$ places to excite the visons and, $O(N^2)$ ways to excite two Bogoliubov quasiparticles. In our study, we drop these contributions, which are small since the overlap $|\langle \Phi'_0 | \Phi_0 \rangle|^2$ is large.

Numerical results for different parameters of the model

QPI due to vison

Vison excitations near a defect cost less energy than in the bulk. This causes the electron LDOS to be ultra-localized near the defect for energies smaller than the bulk energy to excite a pair of visons. In Fig. 1 we plot electron LDOS at $E = 0.13K$ for (a) $t = 10^4 K$ and (b) $t = K$, where QPI is mainly contributed by vison. Interestingly, the QPI due to vison is insensitive to the ratio t/K . In Figs. 1 (c) and (d) we plot the same but for $E = 0.22K$, where again the contribution of the vison dominates. At this energy, the exact three-lobed shape changes slightly, but the majority of the weight is near the defect in both cases.

Near Dirac cone at $t = 10^4 K$

In the main text, we show results for extracting the spinon dispersion near the top of the band, where the dispersion is quadratic. The protocol can be applied at other values of the spinon energy, particularly near the Dirac point. In

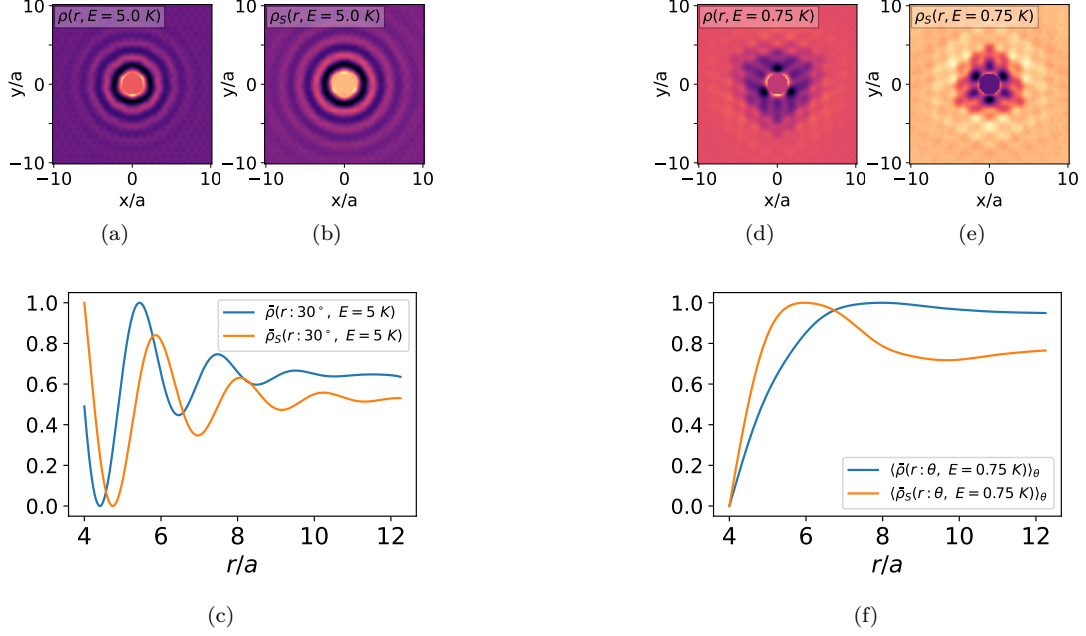


FIG. 3. More results with the parameters $t = K$. Panel (a) shows electron LDOS and (b) spinon LDOS calculated directly from the model [Eq. (6) in the main text] for comparison all at $E = 5.0K$. Visually, they all look similar. Taking a line cut and plotting them on the same graph (c) we see that there is an overall agreement between the electron LDOS and the spinon LDOS. (d)–(f) are the same but for $E = 0.75K$. In this case, there is no direct correspondence between the electron LDOS to the spinon LDOS due to the lack of the separation of electron and spinon energy scale. In (c) the electron LDOS and spinon LDOS are taken along the direction of 30 degrees with respect to the x axis, while in (f), the electron LDOS and spinon LDOS are averaged over all angle around the vacancy.

Fig. 2 we show results of using the same protocol near the Dirac cone. Similar to before, we see that even though the electron LDOS looks featureless [Figs. 2 (a), and (d)], taking a derivative with respect to energy [Figs. 2 (b)], reveals the spinon LDOS [Figs. 2 (c)]. From Fig. 2 (e) we see that the differentiated electron LDOS and spinon LDOS agree well.

Results for QPI at $t = K$

In Fig. 3 we show more results for $t = K$. Remember that t is the electron hopping strength. Using our mean-field treatment, we find that the chargon hopping is strongly renormalized and has a much smaller strength at $0.059t$. This means that even when $t = K$, the spinon bandwidth is much larger than that of the chargon. This makes the situation similar to the case where $t \gg K$, and we should expect electron LDOS to resemble spinon LDOS when $E \gg K$. This is indeed the case as shown in Figs. 3 (a), (b), and (c) for an energy close to the top of the spinon band. Looking at Fig. 3 (c) we see that there is reasonable agreement between the electron LDOS and spinon LDOS, except for an overall shift of the curves in space. This agreement is expected to get better the slower the chargon is. For $E \sim K$, as shown in Figs. 3 (d), (e) and (f), the correspondence between the electron LDOS and spinon LDOS is less clear. This is because the bias energy is not sufficient to sample the whole spinon band, and there is no clear separation between spinon and chargon energy. The electron LDOS depends on the convolution of the spinon and chargon LDOS. Nevertheless, clear spatial oscillation in electron LDOS is visible.